2023

A Critical Role for Staphylococcal Nitric Oxide Synthase in Controlling Flavohemoglobin Toxicity

Ryan M. Singh

Sujata S. Chaudhari

Sasmita Panda

Elizabeth H. Hutfless

Cortney E. Heim

See next page for additional authors

Authors

Ryan M. Singh, Sujata S. Chaudhari, Sasmita Panda, Elizabeth H. Hutfless, Cortney E. Heim, Dhananjay Shinde, Abdulelah A. Alqarzaee, Margaret F. Sladek, Vineet Kumar, Matthew C. Zimmerman, Paul D. Fey, Tammy Kielian, and Vinai Chittezham Thomas

Redox Biology 67 (2023) 102935

Contents lists available at ScienceDirect

Redox Biology

journal homepage: www.elsevier.com/locate/redox

A critical role for staphylococcal nitric oxide synthase in controlling flavohemoglobin toxicity

Ryan M. Singh [a], Sujata S. Chaudhari [a], Sasmita Panda [a], Elizabeth H. Hutfless [a], Cortney E. Heim [a], Dhananjay Shinde [a], Abdulelah A. Alqarzaee [a], Margaret Sladek [a], Vineet Kumar [a], Matthew C. Zimmerman [b], Paul D. Fey [a], Tammy Kielian [a], Vinai C. Thomas [a,*]

[a] Center for Staphylococcal Research, Department of Pathology and Microbiology, University of Nebraska Medical Center, Omaha, NE, 68198-5900, USA
[b] Cellular and Integrative Physiology, University of Nebraska Medical Center, Omaha, NE, 68198-5900, USA

ARTICLE INFO

Keywords:
Staphylococcus epidermidis
Bacterial nitric oxide synthase
Flavohemoglobin
Superoxide
Respiration

ABSTRACT

Most coagulase-negative staphylococcal species, including the opportunistic pathogen *Staphylococcus epidermidis*, struggle to maintain redox homeostasis and grow under nitrosative stress. Under these conditions, growth can only resume once nitric oxide (NO) is detoxified by the flavohemoglobin Hmp. Paradoxically, *S. epidermidis* produces endogenous NO through its genetically encoded nitric oxide synthase (seNOS) and heavily relies on its activity for growth. In this study, we investigate the basis of the growth advantage attributed to seNOS activity. Our findings reveal that seNOS supports growth by countering Hmp toxicity. *S. epidermidis* relies on Hmp activity for its survival in the host under NO stress. However, in the absence of nitrosative stress, Hmp generates significant amounts of the harmful superoxide radical ($O_2^{\bullet-}$) from its heme prosthetic group which impedes growth. To limit Hmp toxicity, nitrite (NO_2^-) derived from seNOS promotes CymR-CysK regulatory complex activity, which typically regulates cysteine metabolism, but we now demonstrate to also repress *hmp* transcription. These findings reveal a critical mechanism through which the bacterial NOS-Hmp axis drives staphylococcal fitness.

1. Introduction

Staphylococcus epidermidis is a human skin commensal that can cause serious invasive infections [1,2]. Members of this species are often linked to the etiology of chronic osteomyelitis as they form persistent biofilms on bone and orthopedic implants [3]. Among the host innate immune effectors that control *S. epidermidis* dissemination, NO is thought to play a prominent role [4]. NO targets redox centers in proteins to exert a broad antimicrobial effect [5]. The immediate physiological consequence of NO on staphylococci is a redox imbalance brought about by the inhibition of terminal cytochrome activity [6]. Unlike the more virulent but closely related *S. aureus* isolates, *S. epidermidis* and other coagulase-negative staphylococci are more vulnerable to NO toxicity as they lack a NO-inducible lactate dehydrogenase that can mitigate the growth-limiting effects of altered cellular redox [6]. Paradoxically, *S. epidermidis* itself harbors a nitric oxide synthase (seNOS) predicted to generate endogenous NO with unknown physiological consequences [7].

Multiple studies have elaborated on the functional significance of bacterial NOS. In *Bacillus subtilis and B. anthracis*, NOS activity contributes to oxidative stress resistance, antibiotic resistance, and pathogenesis [8–10]. Similarly, the inactivation of *nos* in *S. aureus* (saNOS) also makes it more susceptible to hydrogen peroxide (H_2O_2) and adversely impacts its resistance to antibiotics like vancomycin and daptomycin [11]. However, *nos* expression has been observed without added stressors, suggesting that saNOS may perform additional physiological functions [7]. Kinkel et al. reported that saNOS activity might play a physiological role during the transition of *S. aureus* from aerobic to microaerobic environments [12]. The authors proposed that when oxygen levels decrease, endogenous NO produced by saNOS could inhibit cytochrome activity and promote the transfer of electrons from reduced menaquinone to nitrate reductase. This would stimulate the utilization of nitrate (NO_3^-) as an alternate electron acceptor for cellular bioenergetic needs. In their model, endogenous NO is also a source of NO_3^- when it is metabolized by Hmp [12]. In contrast to this model, we previously demonstrated that saNOS activity is essential for aerobic metabolism [7]. We have shown that NO_2^- generated by saNOS stimulates aerobic respiration and facilitates growth during post-exponential

* Corresponding author. Department of Pathology and Microbiology, University of Nebraska Medical Center, Omaha, NE 68198-6495, USA.
E-mail address: vinai.thomas@unmc.edu (V.C. Thomas).

https://doi.org/10.1016/j.redox.2023.102935
Received 6 September 2023; Received in revised form 2 October 2023; Accepted 13 October 2023
Available online 16 October 2023

phase [7]. However, the extent to which these phenotypes are conserved in other staphylococci and the mechanism underlying the growth-enhancing effect of NO_2^- remained unclear.

To address these gaps, we used *S. epidermidis* as a model to investigate the physiological role of seNOS-derived NO_2^-. Compared to *S. aureus*, we show that *S. epidermidis* relies more heavily on *nos* activity for aerobic growth and respiration. The increased dependence on *nos* activity enabled the selection of a *nos* suppressor mutant that effectively restored the growth of the *nos* mutant. The suppressor mutation was mapped to *hmp*. Remarkably, we found a significant increase in *hmp* expression in the *nos* mutant due to reduced levels of NO_2^-. Mechanistically, we show that *S. epidermidis* NO_2^- derived from seNOS activity promotes CymR-CysK complex formation and represses *hmp* expression. This regulatory control over *hmp* enhances the growth of *S. epidermidis* by reducing the production of Hmp-dependent $O_2^{\bullet-}$ radical to non-toxic levels.

2. Results

2.1. seNOS promotes aerobic growth and redox homeostasis in S. epidermidis

To investigate the role of seNOS, we initially monitored growth and glucose consumption of the wildtype strain (WT) and isogenic Δ*nos* mutant. The Δ*nos* mutant displayed a substantial decrease in growth (Fig. 1A), which was reversed upon complementation of *nos* in trans (Supplementary Fig. 1A) and consumed more glucose relative to the WT strain (Fig. 1B). A comparison of the excreted metabolites revealed that glucose was converted to lactate and acetate in the Δ*nos* mutant, whereas acetate was the primary metabolite excreted by the WT (Fig. 1C and D). The increased lactate production by the Δ*nos* mutant indicated a redox imbalance brought about by impaired respiration since redirection of carbon flux through lactate dehydrogenase is an adaptive response *S. aureus* utilizes to regenerate NAD^+ from NADH during aerobic growth [6]. Several additional lines of evidence support this conclusion. First, the cellular redox status determination revealed that

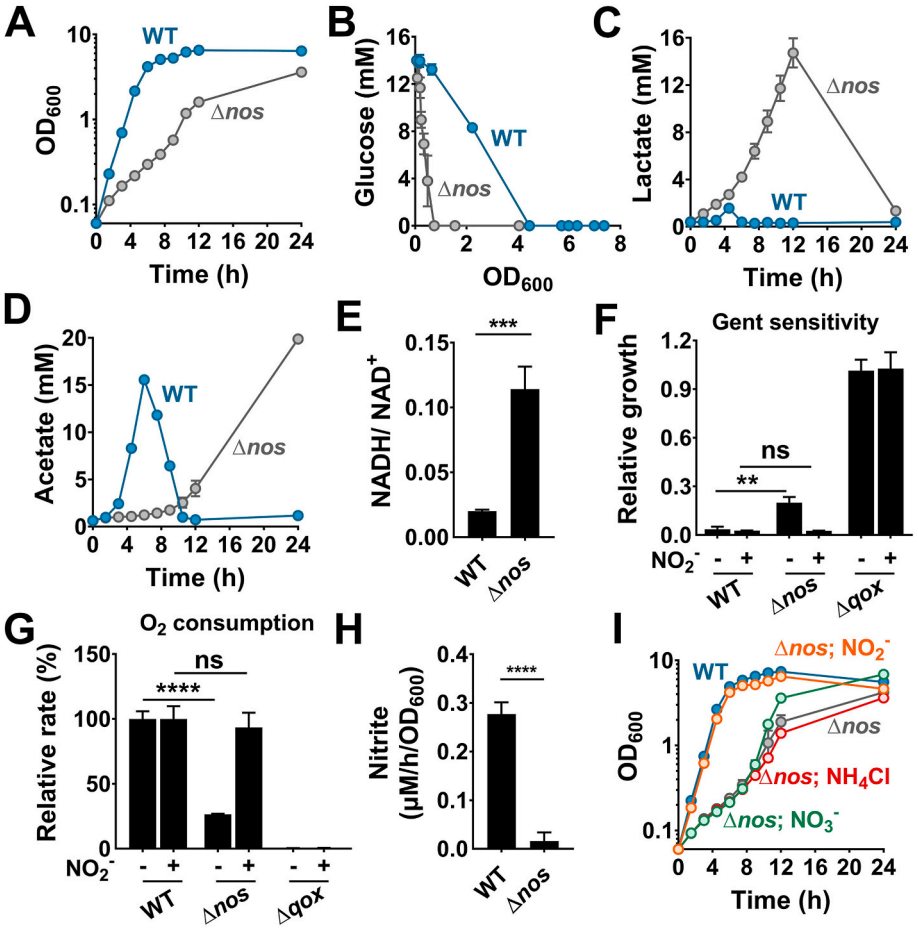

Fig. 1. seNOS-derived NO_2^- activates respiration to sustain growth. **A.** Aerobic growth of the WT and Δ*nos* mutant was measured spectrophotometrically (OD_{600}) following incubation at 37 °C and 250 rpm. **B.** The glucose, (**C**) lactate and (**D**) acetate concentrations were determined from culture supernatants at the indicated times (mean ± SD, n = 3). **E.** The intracellular redox ratio ($NADH/NAD^+$) was measured during the exponential growth phase of strains (mean ± SD, n = 3, Student's *t*-test; $^{***}P \leq 0.0005$). **F.** Gentamicin susceptibility assay. The ratio of the area under the growth curve (AUC) of cultures challenged with 2 μg/ml gentamicin relative to cultures grown in the absence of antibiotic (referred here as relative growth) was determined as the measure of gentamicin sensitivity of bacterial strains (mean ± SD, n = 3, Two-way ANOVA with Sidak's post-comparison test; $^{*}P \leq 0.05$). The Δ*qox* mutant (cytochrome oxidase mutant) with impaired respiration was included as a positive control in the assay. $NaNO_2$ concentration, 1 mM. **G.** Oxygen consumption was determined by measuring the time-resolved fluorescence of the oxygen-sensitive probe (MitoXpress, Luxcell Biosciences) in cultures supplemented with or without 1 mM $NaNO_2$ (mean ± SD, n = 3, Two -way ANOVA with Sidak's post-comparison test; $^{****}P \leq 0.00005$). **H.** Nitrite levels were determined using the Griess assay. The rate of nitrite production was estimated from the total nitrite accumulated in culture supernatants between 3.5 h and 24 h of growth and normalized to the time and OD_{600} (mean ± SD, n = 3, Student's *t*-test; $^{****}P \leq 0.00005$). **I.** The growth profile of the Δ*nos* mutant was determined in cultures containing either 1 mM $NaNO_3$, 1 mM $NaNO_2$ or 10 mM NH_4Cl. Values represent mean ± SD (n = 3).

the Δ*nos* mutant had an increased NADH/NAD^+ ratio relative to the WT (Fig. 1E), consistent with a block in the respiratory chain. Second, compared to the WT strain, the Δ*nos* mutant was more resistant to gentamicin (Fig. 1F), an aminoglycoside antibiotic that requires an active respiration-dependent membrane potential for transport and activity within cells [7,13]. In this bioassay, the Δ*qox* mutant, which respired very poorly (Fig. 1G), was least sensitive to gentamicin (Fig. 1F). Finally, the Δ*nos* mutant had a significantly decreased oxygen consumption rate relative to the WT strain (Fig. 1G), which suggested a reduction in the terminal cytochrome oxidase activity. Together, these findings indicate that the Δ*nos* mutant sustains significant deficits in maintaining redox homeostasis due to poor respiratory capacity, which affects its growth.

2.2. seNOS-derived NO_2^- suppresses Hmp toxicity

Previously, we demonstrated that endogenous NO in *S. aureus* is rapidly oxidized to NO_3^- and NO_2^- [7]. The NO_2^- played a role in activating aerobic respiration [7]. Thus, we next determined if seNOS activity in *S. epidermidis* resulted in NO_2^- production and whether the absence of seNOS function could be bypassed by adding exogenous NO_2^-. Indeed, inactivation of seNOS decreased the rate of NO_2^- production (Fig. 1H), and external supplementation of NO_2^- (but not NO_3^-) under aerobic conditions restored the growth of the *S. epidermidis* Δ*nos* mutant to WT levels (Fig. 1I). Furthermore, although NO_2^- is rapidly converted to NH_4^+ by *S. epidermidis*, external supplementation of NH_4Cl did not rescue the growth defect of the Δ*nos* mutant (Fig. 1I). External NO_2^- supplementation also restored gentamicin sensitivity (Fig. 1F) and respiration of the Δ*nos* mutant to WT levels (Fig. 1G). Thus, NO_2^- alone could bypass the necessity of seNOS during aerobic growth. A dose-response curve for NO_2^- revealed that growth restoration of the Δ*nos* mutant initiated at concentrations as low as 125 μM, with maximum growth observed at 1 mM NO_2^-. The latter concentration is approximately twenty-five times higher than what is observed to fully rescue the *S. aureus nos* mutant [7]. The disparity in NO_2^- concentrations may stem from variations in NO_2^- uptake rates in these strains (Supplementary Fig. 1F).

We next asked how NO_2^- stimulated aerobic growth. Whole-cell EPR spectroscopy, performed using 1-hydroxy-3-methoxycarbonyl-2,2,5,5-tetramethyl pyrrolidine (CMH) as a spin probe, revealed increased reactive oxygen species (ROS) levels in the Δ*nos* mutant relative to the WT strain (Fig. 2A). In these assays, the addition of superoxide dismutase (SOD), but not dimethyl thiourea (DMTU), a hydroxyl ($^\bullet$OH) radical scavenger, significantly quenched ROS signal suggesting that $O_2^{\bullet-}$ comprised the primary component of the observed ROS (Fig. 2A). Furthermore, supplementation of the antioxidant N-acetyl cysteine (Fig. 2B) or growth of the Δ*nos* mutant under anaerobic conditions (Fig. 2C), significantly restored the growth of the Δ*nos* mutant, thus underscoring the toxicity of endogenous ROS produced in the Δ*nos* mutant. Finally, the addition of NO_2^- eliminated ROS production in the Δ*nos* mutant (Fig. 2D). These findings suggest that seNOS-derived NO_2^- suppresses endogenous ROS production, which antagonizes the aerobic growth of *S. epidermidis*.

The production of $O_2^{\bullet-}$ in the Δ*nos* mutant does not result from a decrease in endogenous levels of superoxide dismutase (SOD). Instead, the Δ*nos* mutant had increased SOD activity during the early growth phase relative to the WT strain (Supplementary Fig. 2). To further resolve the source of $O_2^{\bullet-}$ production in the Δ*nos* mutant, we screened for *nos* suppressor mutants whose small colony size reverted to WT colony morphology during growth on tryptic soy agar media. Whole-genome sequencing of eight such suppressors identified a single nucleotide substitution (C→T) in all strains that was predicted to form a truncated variant of the flavohemoglobin Hmp (Q334STOP; (Supplementary Fig. 3A). The production of the truncated Hmp protein variant was verified through tandem mass spectrometry. Targeted analysis of Hmp peptides, released after trypsin digestion of crude cell extracts, was conducted. We observed elevated levels of a distinctive N-terminal Hmp tryptic peptide in the WT, Δ*nos*, and the Δ*nos* suppressor mutants. However, a C-terminal peptide, specific to the truncated region of Hmp, was detected solely in the WT and Δ*nos* mutant, but not in the Δ*nos* suppressor mutants as anticipated (Supplementary Fig. 3A). Furthermore, since the endogenous NO dioxygenase activity of Hmp (conversion of NO to NO_3^- in the presence of O_2) protects bacteria against nitrosative stress [14], we observed that the premature truncation of Hmp increased the susceptibility of all Δ*nos* suppressors to nitrosative stress following S-nitrosoglutathione (GSNO) treatment, confirming a loss of function mutation in *hmp* (Supplementary Figs. 3B and C).

It has been suggested that under substrate-limiting conditions, oxygen may escape from the heme site of Hmp as $O_2^{\bullet-}$ [15,16]. Therefore, we tested whether Hmp-dependent ROS toxicity was enhanced in the absence of seNOS. Whereas mutation of *hmp* alone did not affect growth, the Δ*hmp*Δ*nos* mutant exhibited an almost complete restoration of growth to WT levels (Fig. 3A). Furthermore, complementation of *hmp* in trans decreased the growth rate of the Δ*hmp*Δ*nos* mutant due to increased toxicity (Supplementary Fig. 1B). Additionally, the Δ*hmp*Δ*nos* mutant did not generate endogenous ROS (Fig. 3B), and respiration was restored in this mutant to WT levels (Fig. 3C). To further elucidate the role of Hmp as the source of $O_2^{\bullet-}$ in the Δ*nos* mutant, we engineered mutations in the native chromosomal *hmp* allele that disrupted either its FAD-binding domain ($hmp^{Y202A,\ S203A}$) or heme-binding site (hmp^{H85A}) (Supplementary Fig. 3A) [15]. Whereas the FAD-prosthetic group of Hmp can divert electrons towards the reduction of free iron (Fe^{3+}) in the cytoplasm and contribute to $^\bullet$OH radical generation via Fenton chemistry [15], the heme cofactor of Hmp has been reported to produce $O_2^{\bullet-}$ [16]. Upon challenge with GSNO, we observed that both $hmp^{Y202A,\ S203A}$ and hmp^{H85A} mutants were sensitive to the resulting nitrosative stress,

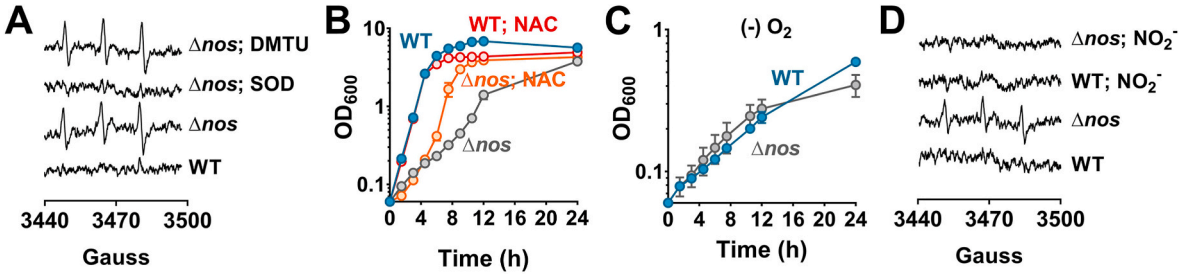

Fig. 2. SeNOS-derived NO_2^- inhibits endogenous $O_2^{\bullet-}$ production. A. Whole cell EPR spectroscopy of the WT and Δ*nos* mutant after 12 h of growth. ROS was detected by EPR spectroscopy using CMH as a spin probe (see Materials and Methods). Superoxide dismutase (SOD, 400 U) and dimethyl thiourea (DMTU, 20 mM) were used as $O_2^{\bullet-}$ and $^\bullet$OH radical scavengers, respectively. Representative traces are displayed, (n = 3). **B.** The growth (OD_{600}) of the WT and Δ*nos* mutant was monitored in the presence or absence of N-acetyl cysteine (NAC, 20 mM). Values represent mean ± SD (n = 3). **C.** The growth (OD_{600}) of the WT and Δ*nos* mutant was monitored under anaerobic conditions at 37 °C and 250 rpm. Values represent mean ± SD (n = 3). **D.** Representative EPR spectroscopic traces of WT and Δ*nos* mutant following growth in media supplemented with or without 1 mM $NaNO_2$, (n = 3).

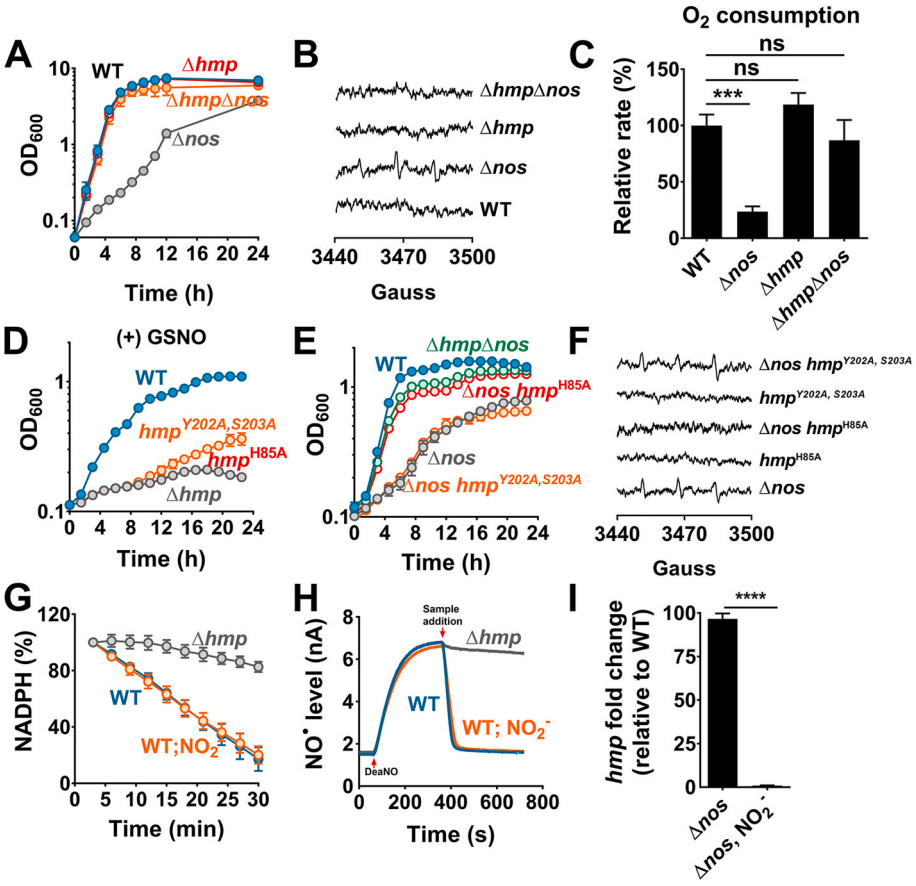

Fig. 3. Hmp is a significant endogenous $O_2^{\bullet-}$ source in the Δ*nos* mutant. **A.** Growth profiles (mean ± SD, n = 3), **(B)** representative EPR spectroscopic traces (n = 3), and **(C)** oxygen consumption rates (mean ± SD, n = 3, One-way ANOVA with Tukey's post-comparison test; ***$P \leq 0.0005$) of the Δ*nos* and Δ*hmp* mutants were determined relative to the WT strain. **D.** The growth of the WT expressing *hmp* variants with altered FAD binding site (*hmp*$^{Y202A,\ S203A}$) or heme binding site (*hmp*^{H85A}) was monitored at OD_{600} following 4 mM GSNO challenge (mean ± SD, n = 3). **E.** The growth (OD_{600}) of the Δ*nos* mutants expressing various *hmp* variants was determined relative to the WT strain (mean ± SD, n = 3). **F.** Representative EPR spectroscopic traces of strains expressing different *hmp* variants (n = 3) **G.** Hmp-dependent NADPH consumption (mean ± SD, n = 3) and, **(H)** NO consumption by cell extracts (250 μg total protein) from various strains were monitored after adding 1 mM $NaNO_2$. DeaNONOate (DeaNO) is used as NO congener. (n = 3). Sample addition indicates the time of addition of cell extract. **I.** Transcription of *hmp* was measured by RT-qPCR following 24 h of growth in the presence or absence of 1 mM $NaNO_2$ (mean ± SD, n = 3, Student's *t*-test; ****$P \leq 0.00005$).

which suggested that both cofactors of Hmp are necessary for efficient NO detoxification (Fig. 3D). However, upon introducing these mutations into the Δ*nos* mutant background, the expression of the Hmp$^{Y202A,\ S203A}$ protein variant was as toxic to growth as the native Hmp suggesting that the FAD-binding domain of Hmp was not the source of ROS in the Δ*nos* mutant (Fig. 3E). Instead, the expression of the Hmp^{H85A} protein variant in the Δ*nos* mutant restored its growth to WT levels (Fig. 3E), indicating that the heme site within Hmp was the source of $O_2^{\bullet-}$ in the Δ*nos* mutant. Indeed, EPR spectroscopy confirmed that the *nos* mutant expressing the Hmp^{H85A} variant no longer generated ROS (Fig. 3F). The observed toxicity of Hmp was also conserved in *S. aureus*, as the growth yield of the *S. aureus nos* mutant was mostly restored to WT levels (Supplementary Fig. 4) following mutation of *hmp* in that background, demonstrating the broader implications of this regulation in staphylococci.

Given that NO_2^- restores the Δ*nos* mutant growth, we predicted that NO_2^- modulates Hmp-dependent $O_2^{\bullet-}$ production. Therefore, we initially tested whether NO_2^- inhibits Hmp activity at the protein level. However, up to 1 mM NO_2^- did not alter the rate of NADPH utilization (Fig. 3G) or NO consumption (Fig. 3H) by Hmp in WT cell extracts compared to untreated samples. However, at the transcriptional level, we observed that the basal expression of *hmp* had increased nearly 97-fold in the Δ*nos* mutant relative to the WT (Fig. 3I). Consistent with this phenotype, cytoplasmic extracts of the Δ*nos* mutant were also able to consume NO faster than WT (Supplementary Fig. 5). Importantly, NO_2^- supplementation reduced *hmp* expression in the Δ*nos* mutant to WT levels (Fig. 3I). These observations suggest that seNOS-dependent NO_2^- production regulates *hmp* transcription.

2.3. Transcriptional control of hmp by seNOS is mediated through the CymR-CysK regulatory complex

Unlike most firmicutes, staphylococci do not have a homolog of the NO_2^-/NO sensitive transcriptional repressor, NsrR, known to regulate *hmp* in other bacteria [17,18]. However, staphylococci possess CymR, an Rrf2 family protein like NsrR, that may be responsive to NO_2^- [19]. In addition, previous studies in *S. aureus* have reported that the *srrAB* two-component system can regulate *hmp* expression during nitrosative stress [20]. Also, a potential role for staphylococcal Rex, the redox sensing transcriptional repressor, is suspected in controlling *hmp* [21]. To determine if any of these transcriptional regulators mediated the NO_2^--dependent restoration of growth in the Δ*nos* mutant, we compared the growth profiles of the Δ*nos* mutant to Δ*rex*Δ*nos,* Δ*srrA*Δ*nos* and Δ*cymR*Δ*nos* double mutants both in the presence and absence of NO_2^- (Fig. 4A–C). While the growth of all double mutants were either similar or poorer than the Δ*nos* mutant when grown in tryptic soy broth (TSB) containing 14 mM glucose, the addition of NO_2^- restored the growth of all but the Δ*cymR*Δ*nos* mutant to WT levels (Fig. 4A–C). This suggested that NO_2^- may regulate *hmp* in a CymR-dependent manner. Consistent with this hypothesis, transcriptional analysis of the Δ*cymR*Δ*nos* mutant

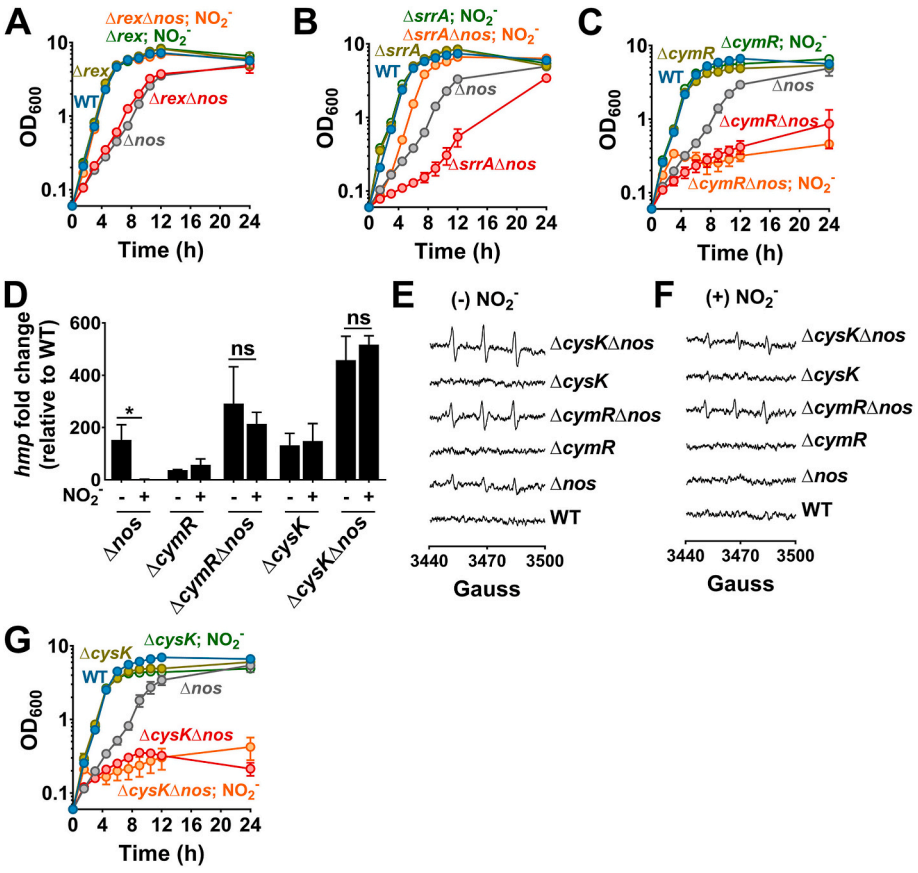

Fig. 4. NO_2^--dependent transcriptional control of *hmp* requires functional CymR and CysK. Growth (OD_{600}) of **(A)** *Δrex*, **(B)** *ΔsrrA* and **(C)** *ΔcymR* mutants in TSB (mean ± SD, n = 3). **D.** The *hmp* expression was measured by RT-qPCR following 24 h of growth (mean ± SD, n = 3, Two-way ANOVA with Sidak's post-comparison test; $^*P \leq 0.05$). Representative EPR spectroscopic traces for the WT and various *cymR* mutants were determined in the **(E)** absence or **(F)** presence of 1 mM $NaNO_2$. (n = 3) **G.** Growth (OD_{600}) of *ΔcysK* mutants in TSB (mean ± SD, n = 3). The concentration of $NaNO_2$ supplemented in cultures, 1 mM.

confirmed that NO_2^- was unable to mediate *hmp* repression (Fig. 4D) or decrease Hmp-dependent $O_2^{\bullet-}$ production (compare Fig. 4E and F) in this mutant. Surprisingly, we also noted that the Δ*srrA*Δ*nos* mutant displayed an enhanced growth defect relative to the Δ*nos* mutant (Fig. 4B), even though *hmp* expression had moderately decreased in this strain (Supplementary Fig. 6A). This is presumably due to the severe respiratory arrest in the Δ*srrA*Δ*nos* mutant (Supplementary Fig. 6B) resulting from its inability to increase *qox* expression [7,22]. The poor growth of the Δ*srrA*Δ*nos* mutant was restored to a Δ*nos* mutant phenotype upon complementation (Supplementary Fig. 1C).

To investigate how seNOS-derived NO_2^- triggers CymR function, we initially explored whether NO_2^- could interact with Cys25, a redox-active site in CymR, thereby regulating *hmp* repression [23]. To address this, we genetically modified both the WT and Δ*nos* mutant strains to produce the $cymR^{C25A}$ variant in place of its native copy. However, expression of the $CymR^{C25A}$ variant did not prevent NO_2^- from restoring the growth of the $cymR^{C25A}$Δ*nos* mutant to WT levels (Supplementary Figs. 7A and B), which suggested that the redox-active cysteine residue in CymR was unlikely to be the target of NO_2^-.

An alternate possibility was that NO_2^- may impact CymR function by influencing its interaction with cysteine synthase (CysK) [24]. As a master regulator of cysteine metabolism in staphylococci, CymR forms a regulatory complex with CysK to transcriptionally repress genes associated with sulfur assimilation, cysteine biosynthesis and cystine uptake in cells (19, 24, 25). When bound to CysK, the DNA binding activity of CymR increases (24, 25). Thus, we hypothesized that seNOS-derived NO_2^- may augment CymR-CysK complex formation to directly repress *hmp* expression. However, to initially test if *cysK* is involved in CymR mediated *hmp* repression, we inactivated *cysK* in the Δ*nos* mutant and determined if NO_2^- still retained its ability to restore growth of this double mutant to WT levels. Remarkably, the Δ*cysK*Δ*nos* mutant phenocopied the growth characteristics of the Δ*cymR*Δ*nos* mutant and was unable to recover its growth in the presence of NO_2^- (Fig. 4G). Moreover, *hmp* expression was elevated in the Δ*cysK*Δ*nos* mutant and NO_2^- was unable to restore *hmp* repression (Fig. 4D) or decrease Hmp-dependent $O_2^{\bullet-}$ production in this strain much like the Δ*cymR*Δ*nos* mutant (compare Fig. 4E and F). Notably, the growth of both the Δ*cymR*Δ*nos* and Δ*cysK*Δ*nos* mutants could be complemented (resensitized to NO_2^-) when either the *cymR* or *cysK* alleles, respectively, were reintroduced into mutants in trans (Supplementary Figs. 1D and E). The above observations indicate that both CymR and CysK are necessary for seNOS-derived NO_2^- to control *hmp* expression.

Given that the regulatory mechanism of CymR-CysK is linked to its capacity to form a heterodimeric complex (CymR2-CysK2) (24), we hypothesized that the reduced endogenous NO_2^- levels in the Δ*nos* mutant may hinder the efficient assembly of the CymR-CysK complex. This would likely result in the derepression of several genes associated with cysteine metabolism in the Δ*nos* mutant (20, 26) and, additionally, increase CysK enzymatic activity, as the latter enzyme is no longer inhibited by complex formation with CymR. Indeed, our findings support these predictions. Transcriptional analysis of multiple genes repressed by the CymR-CysK complex (Supplementary Fig. 8), including *cysI*, *cysJ* (encoding subunits of sulfite reductase), *cysM* (cystathionine β-synthase), *mccB* (cystathionine γ-lyase), and *tcyA* (L-cystine transporter), showed increased expression in the Δ*nos* mutant relative to the WT strain (Fig. 5A). Moreover, NO_2^- supplementation in the Δ*nos* mutant culture restored the repression of these same genes to WT levels (Fig. 5A).

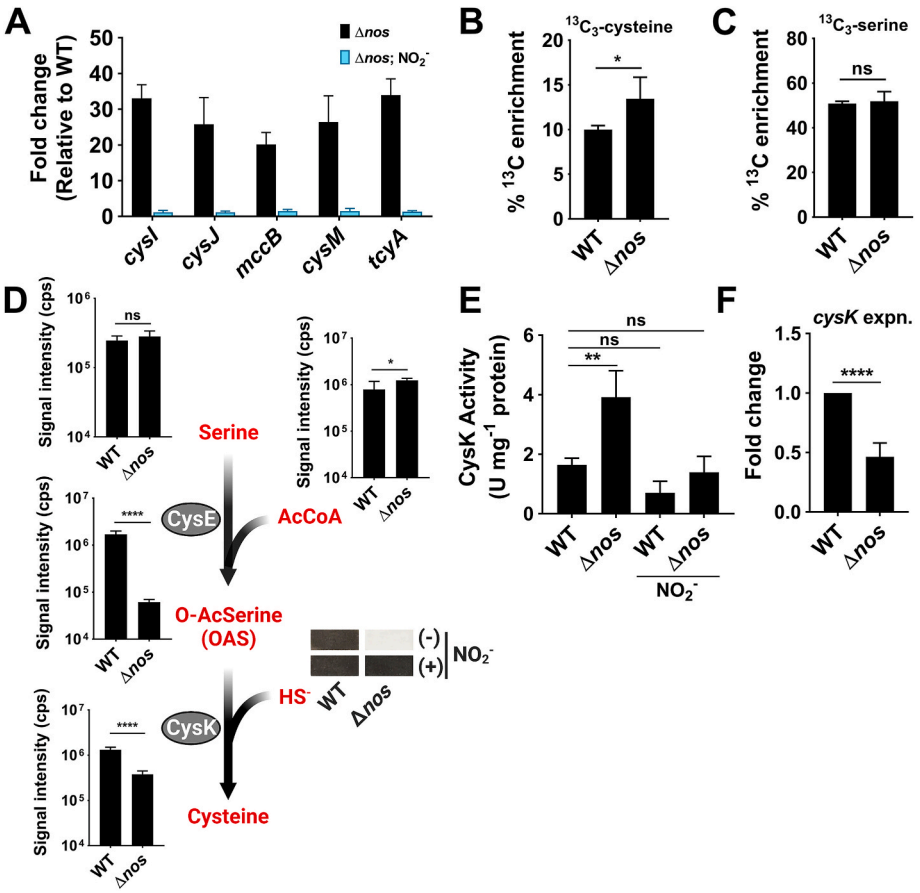

Fig. 5. seNOS-derived NO_2^- promotes the formation of a functional CymR-CysK regulatory complex. A. Transcription of various genes regulated by the CymR-CysK complex was measured in the Δ*nos* mutant relative to WT strain by RT-qPCR following 24 h of growth in TSB ± NO_2^- (mean ± SD, n = 3). The percent ^{13}C enrichment of the M+3 isotopologue of **(B)** cysteine and **(C)** serine in WT and Δ*nos* were determined at metabolic pseudo steady-state following growth in TSB supplemented with 1 mM $^{13}C_3$-serine (mean ± SD, n = 4, Student's *t*-test; $^*P \leq 0.05$). **D.** LC-MS/MS quantitation of various metabolites associated with cysteine biosynthesis, including intracellular serine, acetyl CoA, O-acetyl serine and cysteine, were performed in the exponential phase of growth (OD_{600} of 0.5, mean ± SD, n = 5, Student's *t*-test; $^*P \leq 0.05$ and $^{****}P \leq 0.00005$; cps, counts per second.). Hydrogen sulfide production was measured over 12 h of growth using lead acetate paper in the presence and absence of 1 mM $NaNO_2$ (representative image, n = 3). The formation of lead sulfide results in a dark precipitate on the paper. **E.** CysK activity was assessed in cells grown to exponential phase, both in the presence and absence of 1 mM $NaNO_2$ (OD_{600} of 0.5, mean ± SD, n = 3, One-way ANOVA with Tukey's post-comparison test; $^*P \leq 0.05$) and **(F)** *cysK* gene expression was determined in the exponential phase of growth (OD_{600} of 0.5, mean ± SD, n = 9, Student's *t*-test; $^{**}P \leq 0.005$).

Additionally, flux measurements and direct enzyme activity assays indicated that CysK activity was elevated in the Δ*nos* mutant compared to the WT strain. When cells were fed with $^{13}C_3$-serine, we observed an increased flux of labeled serine towards intracellular cysteine pools under metabolic pseudo-steady state conditions, indicating increased CysK activity (Fig. 5B). The increase in labeled cysteine ($^{13}C_3$-cysteine) in the Δ*nos* mutant did not result from increased $^{13}C_3$-serine uptake, as its levels were comparable in the WT and Δ*nos* mutant (Fig. 5C).

To further validate these findings, we measured the levels of various metabolites associated with the cysteine biosynthetic pathway. We observed that the level of sulfide (H_2S) produced was significantly reduced, as estimated from decreased darkening of lead acetate strips (Fig. 5D). LC-MS/MS analysis showed that O-acetyl serine (OAS), another substrate of CysK, was markedly depleted in the Δ*nos* mutant compared to the WT strain, whereas minimal differences were observed in serine and Acetyl CoA pools (Fig. 5D, see representative peaks in Supplementary Fig. 9). Consistent with a decrease in OAS and H_2S, we found that the CysK enzymatic activity was significantly increased in the Δ*nos* mutant relative to the WT strain (Fig. 5E), despite *cysK* expression being modestly decreased in the Δ*nos* mutant (Fig. 5F). Furthermore, the addition of NO_2^- decreased CysK activity (Fig. 5E) and increased sulfide production in the Δ*nos* mutant to WT levels (Fig. 5D). Since CysK may regain its cysteine synthase activity when it is not bound to CymR, the above findings strongly suggest that in the Δ*nos* mutant, the CymR-CysK regulatory complex is more dissociated compared to the WT strain, and NO_2^- has the capacity to reverse this phenotype.

Next, we conducted electrophoretic mobility shift assays (EMSA) to determine if the CymR-CysK complex can directly bind to the promoter region of the *hmp* gene. In *S. epidermidis*, *scdA* is located immediately upstream of *hmp* and is oriented in the opposite direction (Fig. 6A). The intergenic region between *scdA* and *hmp* contains the promoter elements for both genes. As such, we initially amplified a 274 bp biotin-labeled DNA fragment that encompassed the *scdA-hmp* intergenic region and incubated it with increasing concentrations of the CymR:CysK mixture at a 1:1 M ratio. We observed a concentration-dependent retardation of the *scdA-hmp* intergenic region's mobility by the CymR-CysK complex (Fig. 6B, left panel), which is consistent with a direct interaction between the complex and this region. Furthermore, the gel retardation was reversed when competed with a 200-fold molar excess of unlabeled *scdA-hmp* intergenic region (Fig. 6B, left panel), indicating a high degree of specificity of the CymR-CysK complex for the *scdA-hmp* intergenic region. To identify the location of the CymR-CysK binding site more precisely, we amplified four additional biotinylated DNA segments of varying lengths within the *scdA-hmp* intergenic region (Fig. 6C). EMSAs conducted with these DNA fragments revealed that the CymR-CysK complex directly bound within a 45 bp DNA segment, which includes

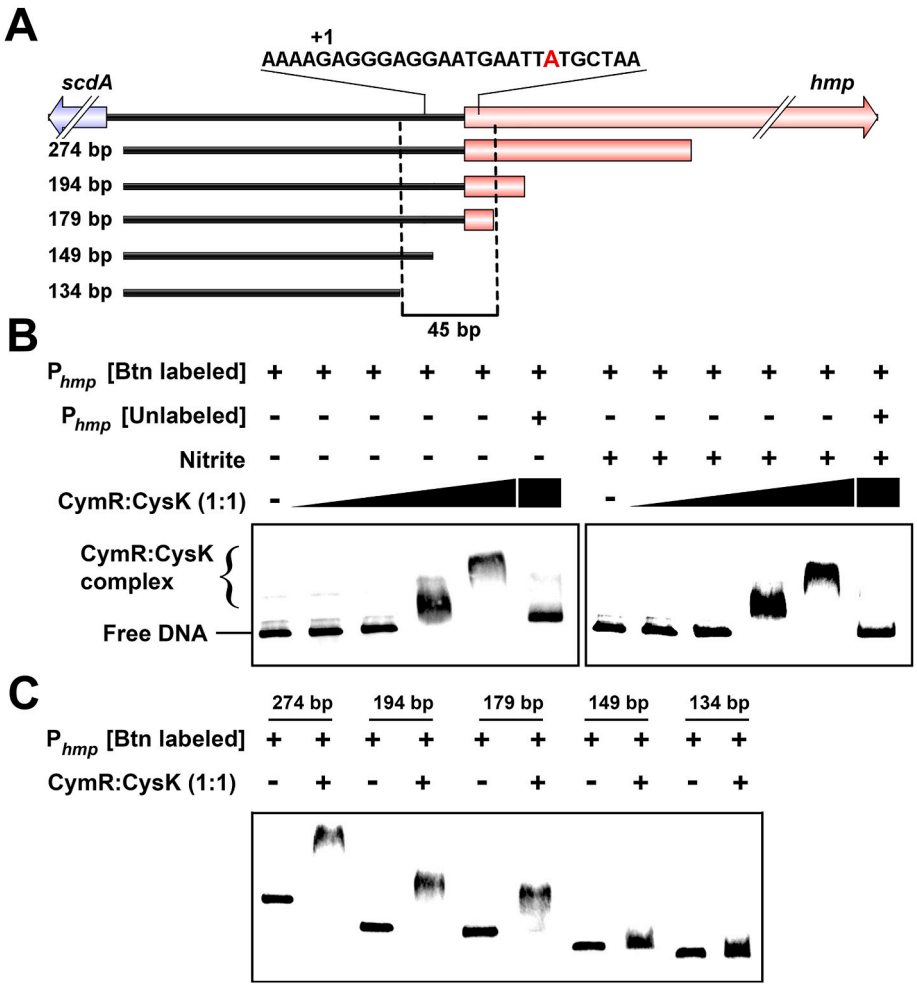

Fig. 6. CymR-CysK regulatory complex binds to the *hmp* promoter. A. Schematic of the *scdA-hmp* intergenic region and various DNA fragments used for EMSA. The vertical dashed lines indicate a 45 bp region where the CymR-CysK complex binds. The DNA sequence presents a potential operator site for CymR-CysK. It includes a transcription start site (+1) identified by adaptor and radioactivity-free method (ARF-TSS) [40], as well as the translation start site ('A' noted in red). **B.** Electron mobility shift assay (EMSA) was performed using a 274 bp biotinylated DNA fragment containing the *hmp* promoter (P_{hmp}). CymR and CysK were mixed in a 1:1 M ratio. The concentration of CymR and CysK varied from 0 (lane1), 0.01 μM (lane2), 0.1 μM (lane 3), 1 μM (lane 4) and 2 μM (lane 5). When noted, 20 fmol of biotin (Btn) labeled P_{hmp} and 200-fold excess of unlabeled P_{hmp} was used in EMSA. The EMSAs were performed either in the absence (left panel) or presence (right panel) of 1 mM $NaNO_2$. **C.** Biotinylated DNA fragments of varying lengths corresponding to different regions within the *hmp* promoter were used to perform EMSA to determine the location of CymR-CysK binding. (For interpretation of the references to color in this figure legend, the reader is referred to the Web version of this article.)

the transcription start site as well as the *hmp* translation start site (compare Fig. 6A–C). The 45-bp region accommodates a motif that resembles a predicted consensus binding site for CymR [25], potentially serving as the operator site (Fig. 6A).

Given that the CymR-CysK complex directly regulates *hmp* expression, we investigated whether NO_2^- stimulates the complex's affinity to bind the *hmp* operator site. However, EMSAs performed with or without added NO_2^- did not reveal significant differences in DNA shift patterns across a range of CymR-CysK concentrations (0.01–2 μM of each protein) (Fig. 6B, right and left panels). These results indicate that NO_2^- does not directly alter CymR-CysK complex's binding affinity to DNA.

A recent study in *S. aureus* demonstrated that Cys85 of CysK is prone to S-nitrosylation by saNOS [26]. Although S-nitrosylation could potentially decrease CysK enzyme activity and thus facilitate its binding to CymR, our investigation did not find supporting evidence for this hypothesis in *S. epidermidis*. Specifically, we examined a Δ*nos* mutant that produced the $CysK^{C85S}$ variant instead of the native CysK enzyme. Despite this alteration, the *cysK*^{C85S}Δ*nos* mutant still responded to NO_2^- and was able to restore its growth defect (Supplementary Figs. 7C and D). These results clearly indicate that Cys85 of CysK is not involved in the response to NO_2^-. Taken together, the above findings suggest that seNOS-derived NO_2^- stimulates CymR-CysK complex formation through an indirect mechanism, ultimately resulting in the direct repression of *hmp*.

2.4. seNOS and Hmp are critical determinants of S. epidermidis pathogenesis

Despite its toxicity, the evolutionary conservation of Hmp and its regulators, including seNOS, CymR and CysK in *S. epidermidis,* would suggest critical roles for these proteins during colonization and infection of the host. Accordingly, we investigated their essentiality during *S. epidermidis* pathogenesis using a mouse model of orthopedic implant biofilm infection. Both Δ*hmp* and Δ*hmp*Δ*nos* mutants were severely attenuated *in vivo*, with significant reductions in bacterial burden in the implant-associated tissue, joint, and femur at day 7 post-infection (Fig. 7A–C). These findings suggest that during an *in vivo* orthopedic infection, *S. epidermidis* Hmp activity is sufficient to diminish host NO to levels that allow growth and survival of this pathogen. Surprisingly, despite the NO-rich infection environment where increased *hmp*

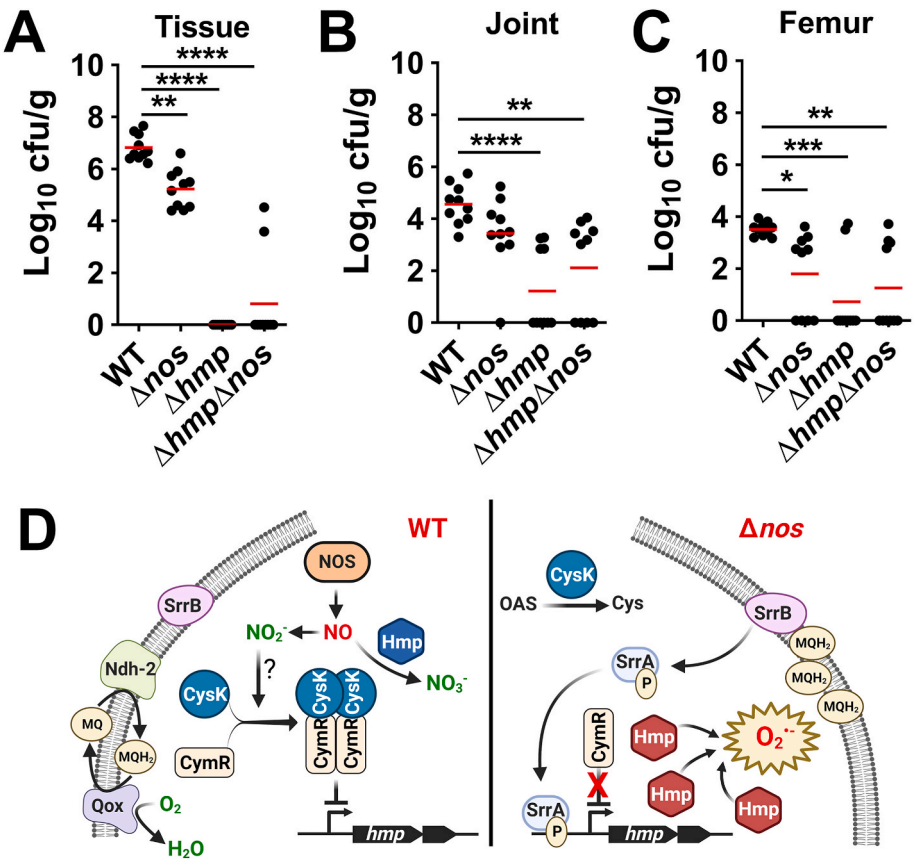

Fig. 7. Hmp and seNOS are required for *S. epidermidis* pathogenesis. Bacterial burdens were determined in the **(A)** tissue, **(B)** joint and **(C)** femur following seven days of infection (red horizontal lines indicate mean, n = 10, One-way ANOVA with Tukey's post-comparison test; $^{*}P \leq 0.05$, $^{**}P \leq 0.005$, $^{***}P \leq 0.0005$ and $^{****}P \leq 0.00005$). **D.** Model depicting the regulatory control of *hmp* by seNOS. NO_2^- is intially formed through the spontaneous oxidation of NO generated by seNOS. The NO_2^- facilitates the formation of the CymR-CysK regulatory complex through a mechanism that remains unknown at this time. The CymR-CysK complex, in turn, directly suppresses *hmp* expression. When *nos* is inactivated (Δ*nos*), CymR-CysK-dependent *hmp* expression and the production of Hmp-dependent $O_2^{\bullet-}$ increase, leading to growth inhibition. Additionally, impaired respiration in the Δ*nos* mutant further amplifies *hmp* expression and toxicity due to the activation of SrrAB signaling. (For interpretation of the references to color in this figure legend, the reader is referred to the Web version of this article.)

expression would be beneficial, titers were also reduced in the Δ*nos* mutant in the tissue and femur relative to WT (Fig. 7A–C). However, the attenuation of the *nos* mutant could result from the pleiotropic effects of a dysfunctional CymR-CysK complex in this strain. Indeed, both the Δ*cymR* and Δ*cysK* mutants were also attenuated most in the tissue and modestly in the joint and femur (Supplementary Fig. 10 A-C). Collectively, these findings are consistent with seNOS signaling through the CymR-CysK regulatory complex during infection and suggest that a delicate balance of seNOS and Hmp activities is crucial for dictating *S. epidermidis* survival *in vivo*.

3. Discussion

The pleiotropic effects of NO and its oxidized products (NO_2^- and NO_3^-) on bacterial physiology suggest multiple functional roles for NOS. In *S. aureus*, at least three distinct functions have been proposed for NOS. These include a role for NOS in oxidative stress resistance [8,9,11,27], the transition from aerobic to hypoxic growth [12], and a role for NOS-derived NO_2^- in stimulating aerobic growth [7]. However, the mechanism associated with the latter function was unclear. Here we utilized *S. epidermidis* 1457 as the model organism to investigate the role of NOS-derived NO_2^- as the *S. epidermidis* Δ*nos* mutant not only exhibited similar phenotypes to those reported in *S. aureus* including impaired respiration, redox imbalance and associated metabolic dysfunction, but also had the added advantage of a more significant growth defect which allowed for the easy screening of suppressor mutants (7). Moreover, when grown in the presence of NO_2^-, the growth defect of the *S. epidermidis* Δ*nos* mutant was almost entirely restored to wild-type levels, consistent with findings in *S. aureus* [7], which allowed for cross-species comparisons and facilitated mechanistic studies.

How, then does NOS-derived NO_2^- stimulate staphylococcal growth? Our findings outline a model (Fig. 7D) wherein NO_2^- limits Hmp-dependent ROS production and toxicity by controlling *hmp* transcription. Hmp toxicity has not been reported in gram-positive bacteria, presumably due to tight transcriptional control and enhanced antioxidant capacity in these organisms. In *S. aureus,* SrrAB activates *hmp* transcription in response to nitrosative stress due to inactivation of terminal oxidases in the electron transport chain [20]. However, a *hmp* repressor like NsrR in *E. coli* has not been identified in *S. aureus*. The presence of a repressor in addition to an activator (SrrAB) would ensure tight transcriptional control of *hmp*. We now show that the CymR-CysK regulatory complex can act as a *hmp* repressor. CymR is an Rrf2 type transcription factor (like NsrR) that is predicted to bind the promoter region as a dimer [28], and act as a global repressor of genes that control cyst(e)ine uptake and biosynthesis [19]. Its affinity for DNA increases several-fold upon interaction with the CysK homodimer. Our findings suggest that in the presence of seNOS-derived NO_2^-, CymR-CysK directly binds to the *hmp* operator site to mediate transcriptional repression. Inactivation of *nos* limits CymR-CysK complex formation, leading to *hmp* expression and toxicity.

While NO typically induces *hmp* expression in bacteria, our research reveals the opposite effect (*hmp* repression) in *S. epidermidis* when NO is

generated through endogenous seNOS activity. This apparent contradiction in observed phenotypes may be attributed to varying NO concentrations. High exogenous NO concentrations, as seen with host iNOS-produced NO, effectively inhibit staphylococcal respiration and activate *hmp* via SrrAB signaling. In contrast, the lower concentrations produced by endogenous seNOS are effectively converted to nitrite, which, in turn, supports respiration and promotes *hmp* repression through CymR-CysK regulation.

The stability of the CymR-CysK complex has been found to correlate with the concentration of its substrate, OAS (26). When cellular cysteine levels are diminished, OAS accumulates, prompting the dissociation of the CymR-CysK complex (26). Consequently, CysK (cysteine synthase) becomes unbound and presumably facilitates the conversion of OAS into cysteine. Subsequent reduction in the OAS pool might permit CysK to associate with CymR once again, thus reestablishing transcriptional control over its regulon. Intriguingly, even though intracellular OAS levels are low in the Δ*nos* mutant, the regulatory influence of the CymR-CysK complex on its regulon remains deficient. This suggests the existence of additional molecular factors influencing CymR-CysK complex formation *in vivo*, rendering the process more complex than previously assumed.

We previously determined that a decreased respiratory capacity of the Δ*nos* mutant due to poor quinol oxidase activity is responsible for SrrA activation in *S. aureus* JE2 [7]. These findings were later confirmed in *S. aureus* UAMS-1 [29]. Notably, we observed a similar loss of respiratory potential and SrrA activation in the *S. epidermidis* Δ*nos* mutant. Indeed, the inactivation of *srrA* severely impaired the growth of the Δ*nos* mutant, consistent with SrrA being active upon *nos* inactivation. In addition, we found that *hmp* transcription modestly decreased in the Δ*nos* mutant following *srrA* inactivation. Thus, in addition to the role of CymR-CysK, our data suggest that SrrA contributes to the overall increase in *hmp* expression in the Δ*nos* mutant due to impaired respiration.

Previous studies have reported Hmp-dependent ROS production in gram-negative pathogens like *E. coli* and *Salmonella* [15,16,30]. However, the exact nature of these oxygen radicals has been questioned. Hmp has two sites that could generate ROS: the flavin and heme centers. Early studies using purified Hmp suggested that in the absence of NO, the oxygen bound to the heme-iron escapes as $O_2^{\bullet-}$ upon reduction [31,32]. Consistent with this prediction, the overexpression of *hmp* activated SOD transcription in *E. coli* [16]. Also, *nsrR* mutants of *Salmonella* that overproduced Hmp were susceptible to $O_2^{\bullet-}$ and peroxide stress [33]. In contrast, Bang et al. determined that the loss of electrons from the flavin center of Hmp, rather than heme, caused Hmp toxicity in *Salmonella* [15]. These electrons released from FAD would eventually contribute to the formation of harmful $^{\bullet}OH$ radical through Fenton chemistry [15]. However, in *S. epidermidis*, our findings support $O_2^{\bullet-}$ as the primary ROS produced by Hmp since disruption of the seNOS heme-binding site, but not the FAD site, alleviated Hmp cytotoxicity. It is conceivable that endogenous $O_2^{\bullet-}$ and its downstream derivatives, H_2O_2 and $^{\bullet}OH$ radical, could all contribute to cytotoxicity.

The mechanisms responsible for the significant decrease in respiration following *nos* mutation have yet to be identified. One potential explanation for reduced respiration could be linked to an adaptive response in the Δ*nos* mutant aimed at limiting the production of $O_2^{\bullet-}$ from the electron transport chain. Alternatively, decreased respiration observed in the Δ*nos* mutant might result from oxidative damage of membrane components, which might negatively impact cytochrome activity. Regardless of the specific mechanism, our findings suggest that reduced respiration leads to a redox imbalance in the Δ*nos* mutant, characterized by elevated NADH/NAD + ratio. The increased NADH level likely serves as a source of electrons for Hmp within the Δ*nos* mutant, contributing to Hmp-dependent $O_2^{\bullet-}$ production.

Traditionally, *S. epidermidis* has been viewed more as a skin commensal than a pathogen [1]. The inability of *S. epidermidis* to adapt to host immune threats that disrupt bacterial redox homeostasis, and the lack of established virulence factors contribute to this perspective [1,6]. However, *S. epidermidis* can develop medical device-associated biofilm infections in humans, frequently observed in the hospital setting [1]. The attenuated phenotypes of the Δ*hmp,* Δ*nos,* Δ*cymR* and Δ*cysK* mutants in a mouse orthopedic biofilm model suggest that these proteins play essential roles in *S. epidermidis* pathogenesis. In humans, the ability of staphylococci to survive on the skin and other host niches differentially expose it to host NO [34]. Our data suggest that while Hmp is an efficient enzyme for NO detoxification and crucial for staphylococcal survival *in vivo*, its dysregulated expression exerts a fitness cost that appears to be evolutionarily countered by the acquisition of NOS. These findings highlight an important and novel mechanism by which staphylococcal NOS and Hmp interact to promote fitness.

4. Materials and Methods

4.1. Bacterial strains, plasmids, and growth conditions

Staphylococcal strains were grown aerobically at 37 °C with agitation at 250 rpm in Tryptic Soy Broth (TSB) containing 14 mM glucose. The growth (OD_{600}) of cultures was monitored in 25 ml volumes with a flask-to-volume ratio of 10:1 over a period of 24 h. For automated analysis of culture densities (OD_{600}) in a 96-well microtiter plate, the Tecan Infinite M200 spectrophotometer was employed. When cells were grown in the 96-well microtiter plates, the maximum aeration setting and a temperature of 37 °C were used. Detailed information about the bacterial strains, vectors, and primers used in this study can be found in Supplementary Tables 1, 2, and 3, respectively. *E. coli* was cultured in Luria Bertani (LB) broth. As needed, the following antibiotics were added to cultures: ampicillin (100 μg/ml), gentamicin (2 μg/ml), anhydrotetracycline (100 ng/ml), and chloramphenicol (10 μg/ml). Additionally, specific growth media were supplemented with various compounds, including sodium nitrate (1 mM), sodium nitrite (1 mM), ammonium chloride (10 mM), GSNO (4 mM), and N-acetyl cysteine (20 mM). To assess gentamicin sensitivity, the relative growth was determined as the ratio of the area under the growth curve (AUC) of gentamicin-treated strains to that of the corresponding untreated control. Calculating the AUC after gentamicin treatment provided valuable insight into how the antibiotic impacted overall bacterial growth. However, to account for any inherent growth defects in specific mutants, the effects of the antibiotic on bacterial growth needed to be normalized to the AUC of the same bacterial culture grown without antibiotics. This normalization allowed us to negate the impact of any growth differences unrelated to the antibiotic treatment.

4.2. Bacterial growth rate determination

The growth rate was determined by creating a plot of the natural logarithm of the optical density (OD_{600}) of bacterial cultures over time. The specific growth rate (μ) was then calculated from two time points selected from the exponential growth phase using the following formula:

$$\mu = (\mathrm{Ln\ OD2} - \mathrm{Ln\ OD1}) / \Delta t$$

where OD2 and OD1 are the optical densities at time t2 and t1, and Δt is the time interval between the t2 and t1.

4.3. Construction and complementation of mutants

In-frame markerless gene deletions in *S. epidermidis* were engineered using a temperature-sensitive vector, pJB38, as described previously [35]. Briefly, the upstream and downstream DNA sequences flanking the genes targeted for deletion were cloned into the multiple cloning site of pJB38. The resulting vectors were electroporated into the restriction-deficient intermediate strain *S. aureus* PS187 Δ*hsdR*Δ*sauUSI* and phage-transduced into *S. epidermidis* 1457 using Φ187 [36]. The *S. epidermidis* 1457 colonies containing pJB38-derivatives were selected

on TSA containing chloramphenicol (10 μg/ml) at 30 °C. Next, the plasmids were integrated into the chromosome of *S. epidermidis* 1457 by inducing homologous recombination at 45 °C to generate single recombinants and selected on TSA containing chloramphenicol (10 μg/ml). Subsequently, single recombinants were serially subcultured thrice in TSB at 30 °C to promote plasmid excision from the chromosome and plasmid curing. The resulting cultures were plated on TSA containing anhydrotetracycline (2 ng/ml) and incubated at 30 °C (counter-selection) to enrich for those colonies that were cured of the plasmid. Finally, a subset of the colonies was screened by PCR using primers flanking the cloning region to identify strains with the engineered mutation from those that retained the WT allele. Chromosomal point mutations resulting in the expression of *hmp* and *cymR* variants were also generated using pJB38. To achieve this, primers with the desired point mutations were used to amplify the *hmp, cymR* and *cysK* alleles. Subsequently, the PCR fragments containing these point mutations were cloned into pJB38, and the allelic exchange process was performed as described above.

Some *S. aureus* mutants described in this study (Table S1) were obtained from the Nebraska Transposon Mutant Library (NTML). However, the transposon mutations were transduced back into the *S. aureus* JE2 strain background using Φ11 [7]. This step is commonly carried out to eliminate any off-target mutations that may have inadvertently been present in the NTML strain.

Complementation of the Δ*nos,* Δ*srrA,* Δ*hmp,* Δ*cymR*, and Δ*cysK* mutants in *S. epidermidis* was performed *in trans* by cloning the full-length *genes* under the control of their native promoter in plasmid pLI50. The plasmid was electroporated into the respective mutants, and the resulting colonies were selected on TSA containing 10 μg/ml chloramphenicol.

4.4. Extracellular metabolite analysis

Glucose, lactate, and acetate concentrations in culture supernatants were determined using commercial kits (R-Biopharm) per the manufacturer's instructions. NAD and NADH were measured using a commercial kit (Promega, #G9072) according to the manufacturer's instructions. Sulfide production by staphylococci was detected using lead acetate paper, as previously described [27]. The lead sulfide (black precipitate) formed from the reaction of sulfide with lead leads to the darkening of the lead acetate paper (Merck, #109511). Nitrite was determined using a commercially available Griess assay kit (Thermo Scientific, #G7921). The nitrite production rate of various strains was estimated by measuring the total nitrite excreted in culture supernatants between 3.5 h and 24 h of growth. The nitrite concentration at these selected growth points was well above this assay's detection limit (1 μM). The difference in nitrite concentrations between these two time points was further normalized to the corresponding change in OD_{600} (growth) and then divided by 20.5 h to estimate the nitrite produced per OD_{600} per hour.

4.5. Targeted metabolite analyses using LC-MS/MS

To extract intracellular metabolites for LC-MS/MS analysis, 20 ml of exponential phase cultures (OD_{600} of 0.5) were withdrawn and mixed with an equal volume of ice-cold saline. The cells were centrifuged in the cold (4 °C) at 10,000×*g* for 5 min and the supernatants were discarded. The pellets were washed in ice-cold saline before being suspended in a 1 ml extraction solution containing 60 % ethanol, 20 % 10 mM ammonium formate, 25 mM NEM and 1 mM Br-ATP as the internal standard. The cells were mechanically lysed in a bead beater set to 6800 rpm and 4 °C (3 cycles of 30 s each with intermittent cooling). The cell debris was separated by centrifugation and the supernatants were stored at −80 °C for metabolite analysis.

Chromatographic separation was performed using an XBridge Amide 3.5 μm (2.1 × 100 mm) column from Waters. Mobile phase A consisted of 10 mM ammonium acetate and 10 mM ammonium hydroxide in water with 5 % acetonitrile, while mobile phase B contained 100 % acetonitrile. The flow rate was set at 0.3 mL/min, and a gradient mode of mobile phases was used. The column was maintained at a constant temperature of 40 °C during the analysis. To prevent any potential sample carryover during separation, we included blanks periodically between samples.

For targeted detection and quantitation of metabolites, a QTRAP 6500+ mass spectrometer (SCIEX) was used in multiple reaction monitoring mode (MRM). The QTRAP6500+ was operated in positive polarity mode for the relative quantitation of amino acids. Electrospray ionization (ESI) parameters were optimized as follows: electrospray ion voltage of 5500V in positive mode, source temperature of 400 °C, curtain gas of 35, and gas 1 and 2 of 40 arbitrary units each. Compound-specific parameters were individually optimized for each metabolite using manual tuning. These parameters include declustering potential (DP) at 65V, entrance potential (EP) at 10V, and collision cell exit potential (CXP) maintained at 10V. The specific MRM transitions for the selected metabolites were as follows: ^{13}C-serine (109.1/62, collision energy CE: 15.5V), serine (106.1/60, CE: 15.5V), NEM_^{13}C-cysteine (250.1/158, CE: 20.0V), NEM_cysteine (247.1/230.1, CE: 11.0V), O-acetylserine (147.9/106.1, CE: 12.0V), and Acetyl CoA (810.2/303.2, CE: 45V).

The final calibration curves for each metabolite were assessed for linearity using linear regression. Peak areas of each metabolite were normalized with the peak areas of the internal standard (8-Br-ATP, CAS# 81035-56-5). These normalized peak areas are presented as relative quantitation values to facilitate interpretation and comparison across the sample groups. The calibration curves are included in Supplementary Fig. 9 to provide a visual representation of the linearity for each metabolite.

4.6. Electron Paramagnetic Resonance spectroscopy

EPR analysis was carried out as previously described with minor modifications [7]. Briefly, 12-h-old stationary-phase bacterial cells were resuspended to an OD_{600} of 10 units in 1 ml of KDD buffer (Krebs-HEPES buffer [pH 7.4]; 99 mM NaCl, 4.69 mM KCl, 2.5 mM $CaCl_2$, 1.2 mM $MgSO_4$, 25 mM $NaHCO_3$, 1.03 mM KH_2PO_4, 5.6 mM D-glucose, 20 mM HEPES, 5 μM diethyldithiocarbamic acid sodium salt [DETC], 25 μM deferoxamine). Then, the bacterial samples were mixed with 200 μM cell-permeable ROS-sensitive spin probe 1-hydroxy-3-methoxycarbonyl-2,2,5,5-tetramethyl pyrrolidine (CMH; Noxygen Science Transfer and Diagnostics, Elzach, Germany) and incubated for 15 min at ambient temperature. EPR analysis was carried out using a Bruker e-scan EPR spectrometer with the following settings: field sweep width, 60.0 G; microwave frequency, 9.75 kHz; microwave power, 21.90 mW; modulation amplitude, 2.37 G; conversion time, 10.24 ms; time constant, 40.96 ms. When appropriate, SOD (400 U) (superoxide dismutase) and DMTU (20 mM) (dimethyl thiourea, a hydroxyl ($^{\bullet}$OH) radical scavenger) were added to bacterial cultures 15 min before CMH.

4.7. Oxygen consumption

S. epidermidis cultures were grown aerobically at 37 °C in 25 ml Tryptic Soy Broth (TSB) supplemented with 14 mM glucose. Samples were collected during the exponential phase, with a collection time of 3.5 h for the WT strain and 6 h for the Δ*nos* and Δ*qox* mutants. The samples were then diluted to an OD_{600} of 0.1 units in sterile saline and aliquoted into the wells of a 96-well plate (150 μl per well).

To determine the oxygen consumption rates of the various strains, a MitoXpress Xtra oxygen-sensitive fluorescent probe from Agilent (#MX-200-4) was used following the manufacturer's instructions. Time-resolved fluorescence measurements were determined on a TECAN M200 spectrophotometer with the following settings: Excitation/Emission wavelengths of 380 nm/650 nm, an optimal delay (lag time) of 30 μs, and an integration time of 100 μs The oxygen consumption rate for

each strain was calculated from the slope and expressed as percentage relative to the parental strain.

4.8. Quantitative reverse-Transcriptase PCR (RT-qPCR) analysis

RT-qPCR was performed as described previously [7]. Briefly, cDNA was synthesized from 500 ng of total RNA using the Quantitect Reverse Transcription Kit (Qiagen, #205313). The cDNA samples were then diluted to 1:20 in double-distilled water and used as a PCR reaction template. The PCR amplification was carried out using the LightCycler DNA Master SYBR green I kit (Roche Applied Science, #12239264001), following the manufacturer's protocol. The relative transcript levels were calculated using the comparative threshold cycle (C_T) method [37] and normalized to the amount of housekeeping sigma factor A (*sigA*) transcripts present in the RNA samples.

4.9. Enzyme activity assays

Total SOD activity from cytoplasmic extracts was determined using a kit (Sigma Aldrich, #19160) per the manufacturer's instructions.

Hmp activity from cytoplasmic extracts was determined by following NO consumption using a NO electrode (World Precision Instruments, Sarasota, FL). Briefly, 80 ml of exponential phase cultures were lysed by bead beating following resuspension of cells in 800 μl lysis buffer containing 0.5 mM EDTA, 2 μM FAD, 1 mM DTT, 1X EDTA-free protease inhibitor cocktail (Roche) and 50 mM PO_4 buffer, pH 7.4. NO was generated within a 1 mL reaction mix containing 0.3 mM EDTA, 100 μM NADPH and 100 mM PO_4 buffer, pH 7.4, by adding 30 μl DeaNONOate (1 mM). Following the stabilization of NO levels in the reaction mix, its consumption was initiated by adding 25 μl of clarified cell extracts (250 μg total protein) and monitored using an NO electrode (ISO–NOP, World Precision Instruments).

Hmp activity was also determined by measuring NO-dependent NADPH consumption [38]. The reaction was initiated by the addition of cell extracts (50 μg total protein) in 100 μl of lysis buffer containing 0.5 mM EDTA, 2 μM FAD, 1 mM DTT, 1X EDTA-free protease inhibitor cocktail (Roche), 250 μM Spermine NONOate, 100 μM NADPH and 50 mM PO_4 buffer, pH 7.4. The NADPH consumption was monitored at 340 nm for 20 min. Cell extracts from Δ*hmp* mutant were used as the negative control in both assays. When required, nitrite was added to a final concentration of 1 mM in the reaction mix to measure its effects on Hmp activity.

CysK enzyme activity was determined colorimetrically as the amount of cysteine formed in a reaction mixture [39]. Briefly, 25 ml of exponential phase cultures grown in the presence or absence of 1 mM $NaNO_2$ were lysed by bead beating following resuspension of cells in 1 ml lysis buffer containing 50 mM phosphate buffer pH 7.5, 10 μM pyridoxal phosphate (PLP), and 1 mM DTT. After lysis, cell free crude extracts containing 10 μg protein were added to a reaction mixture containing 10 mM O-acetylserine (OAS), 5 mM Na_2S, 5 mM DTT and 100 mM HEPES, pH 7.2. The reaction was carried out in a total volume of 100 μl and allowed to continue for 5 min in a water bath adjusted to 37 °C. The reaction was stopped by the addition of 50 μl of 20 % (v/v) trichloroacetic acid (TCA) and then centrifuged at 16,000×*g* to separate reaction supernatant from any protein precipitate. The concentration of cysteine in the reaction supernatant was determined by adding 100 μl of glacial acetic acid and 200 μl of a ninhydrin solution (0.12 g ninhydrin in 3 ml glacial acetic acid and 2 ml 37 % HCl) to 150 μl of the reaction mixture. The mixture was then boiled at 100 °C for 5 min. After cooling, the color was further developed by adding 550 μl of 100 % ethanol and the absorbance was measured at 560 nm. One unit of CysK enzyme activity corresponded to the formation of 1 μmol of cysteine per minute.

4.10. CymR and CysK protein purification

The *cymR* and *cysK* open reading frames were cloned into pET28a vector to generate N-terminal 6 × His tag fusion proteins using primers mentioned in Table S3, before being transferred into BL21(DE3)pLysS and BL21(DE3), respectively. Expression of CymR was induced by adding 1 mM of isopropyl-1-thio-β-D-galactopyranoside (IPTG) to a 200 ml culture grown up to an OD_{600} of 0.6, for 5 h at 30 °C. Purification of CysK was performed following autoinduction of *cysK* for 18 h at 37 °C. Bacterial cells were collected by centrifugation in a Sorvall centrifuge at 10,000 rpm for 10 min at 4 °C. The pellet was resuspended in lysis buffer containing 50 mM sodium phosphate buffer (pH-8.0), 300 mM NaCl, 5 mM Imidazole and passed thrice through an Emulsiflex at 15,000 lb/in^2. The sample was centrifuged at 99,000×*g* for 1 h, and the recombinant protein was purified from the supernatant fraction using a HisPur cobalt resin column per the manufacturer's instructions (Thermo Fischer Scientific). The protein fractions were then dialyzed in 50 mM sodium phosphate buffer (pH-8.0). The purification of proteins was monitored by SDS-PAGE and the concentration was determined by performing Braford assay (Bio-Rad).

4.11. Electrophoretic-linked mobility shift assay (EMSA)

The promoter region of the *hmp* was amplified using biotin-labeled primers mentioned in Table S3 and chromosomal DNA isolated from *S. epidermidis* 1457. The shift assays were performed using LightShift Chemiluminescent EMSA kit (Pierce, #20148) according to the manufacturer's protocol. Briefly, 20 fmol of labeled promoter fragments were incubated at room temperature for 20 min with various amounts of purified proteins in a 20 μl reaction mixture containing 1x binding buffer, 50 ng/ml, 2.5 % glycerol, ploy dI-dC, and 0.05 % NP-40. When mentioned, 4 pmol of unlabeled *hmp* promoter fragments were used as a cold probe. The reaction mixture was loaded on a 5X TBE native PAGE gel at 100V for 1 h and transferred to a nylon membrane (Biodyne™ B Nylon Membrane, Thermo Fisher Scientific). The membrane was crosslinked using auto crosslinking settings on a UV crosslinker (UV Stratalinker 1800) for 1 min. The migration of biotin-labeled promoters was then visualized by using streptavidin-horseradish peroxidase conjugate on a gel documentation system (Thermo Fisher Scientific) using chemiluminescent settings.

4.12. Transcription start-site identification for hmp

The transcriptional start site of hmp was determined by employing the adaptor- and radiation-free identification of transcriptional start site (ARF-TSS) method, as described previously [40]. In brief, 1 μg of RNA isolated from Δ*nos* mutant (where *hmp* expression was upregulated) was subjected to reverse transcription by using 5′-phosphorylated primer hmp_SE_TSS_R1 and first strand cDNA synthesis kit (Invitrogen, Superscript III First-Strand Synthesis System, # 18080-051). RNA was degraded by using 1 M NaOH at 65 °C for 30 min and then neutralized with 1 M HCl. The resultant cDNA was ligated by using T4 RNA Ligase I (Thermo Scientific, # EL0021) to form a circular cDNA. Two inverse primers: hmp_SE_TSS_R2 and hmp_SE_TSS_F3 were used to amplify the circular cDNA. The amplified product was cloned into a TOPO Cloning vector and then sequenced using M13F(-20) and M13R primers. All the primers used in this procedure are mentioned in Table S3.

4.13. Mouse orthopedic implant infection

To model infectious complications in patients following arthroplasty, a mouse model of orthopedic implant biofilm infection was used as previously described [41]. Briefly, mice were anesthetized with ketamine/xylazine (100 mg/kg and 5 mg/kg, respectively) and a medial incision was created through the quadriceps with lateral displacement to access the distal femur. A burr hole was created in the femoral intercondylar notch using a 26-gauge needle to facilitate the insertion of a pre-cut 0.8 cm orthopedic-grade Kirschner wire (0.6 mm diameter, Nitinol [nickel-titanium]; Custom Wire Technologies, Port Washington,

WI) into the intramedullary canal, leaving ~1 mm protruding into the joint space. The exposed wire was inoculated with 10^3 CFU of WT, Δ*nos*, Δ*hmp*, Δ*hmp*Δ*nos,* Δ*cymR* or Δ*cysK* in 2 μl of PBS and the skin was sutured closed. For pain relief, animals received Buprenex (0.1 mg/kg s.c.; Reckitt Benckiser Health Care, Hull, North Humberside, United Kingdom) immediately after infection and 24 h later. After this interval, mice exhibited normal ambulation and no discernible pain behaviors. Animals were sacrificed on day 7 post-infection using an overdose of inhaled isoflurane, after which bacterial burden in the implant-associated soft tissue, joint, and femur were quantified by plating on blood agar plates.

4.14. Whole-genome sequencing

Genomic DNA (1 ng) from various strains was tagmented, amplified, cleaned and bead-normalized using the Nextera XT DNA Library Prep kit (Illumina, #FC-131-1096). The strain-specific DNA libraries were pooled in equal volumes. The pooled libraries and sequencing control (PhiX) were independently diluted and denatured to a final concentration of 20 pM. 10 % PhiX was added to the final pool and then heated at 96 °C for 3 min to ensure complete denaturation before sequencing. Whole-genome sequencing was performed on a MiSeq platform (Illumina) using read length 2x300 bp and onboard fastq file generation and sample demultiplexing. Sequencing reads were analyzed on the CLC Genomics Workbench (Qiagen). The average genome coverage was 65-90x. Single nucleotide variations (SNV) in the suppressors were identified by comparing their sequence to an isogenic parental control.

4.15. Targeted analysis of Hmp using LC-MS/MS

The full-length and truncated Hmp protein variant was distinguished by LC-MS/MS analysis. For sample preparation, cells were grown up to the exponential phase and then treated with 6 mM GSNO for 1 h to increase the intracellular pool of Hmp. At this time, 20 OD_{600} units of cells were collected, centrifuged, and resuspended in sterile saline. The cells were then mechanically lysed in a bead beater set to 6800 rpm and 4 °C (3 cycles of 30 s each). The cell debris was separated by centrifugation and the protein concentration in supernatants was estimated using a Bradford protein assay kit (Bio-rad, #5000006). Next, 100 μg of proteins from each sample was diluted to 100 μL with 100 mM ammonium bicarbonate. The proteins were reduced with 5 μL of 200 mM tris(2-carboxyethyl) phosphine (TCEP) (1 h incubation, 55 °C) and alkylated with 5 μL of 375 mM iodoacetamide (IAA) (30 min incubation in the dark, room temperature). The reduced and alkylated proteins were purified by acetone precipitation at −20 °C overnight. The resulting protein precipitates were collected by centrifugation at 8000×*g* for 10 min at 4 °C and pellets were briefly air-dried and resuspended in 100 μL of 50 mM ammonium bicarbonate. The protein digestion was carried out using 2.5 μg of trypsin per sample (16 h incubation, 37 °C). The digested protein samples were dried under vacuum and then desalted with C18 spin columns (Pierce). Clean peptides were dried under vacuum, resuspended in 0.1 % formic acid, and analyzed using high-resolution mass spectrometry.

For LC-MS/MS, 1.5 μg of each sample was loaded onto trap column Acclaim PepMap 100 (75μm × 2 cm C18 LC Columns, Thermo Fisher Scientific) at a flow rate of 4 μl/min and separated with a Thermo RSLC Ultimate 3000 (Thermo Fisher Scientific) coupled with Orbitrap Fusion Lumos Tribrid Mass Spectrometer on a Thermo Easy-Spray PepMap RSLC C18 column (75μm × 50 cm C-18 2 μm, Thermo Fisher Scientific) at a flow rate 0.3 μl/min and 50 °C, with a step gradient of 9%–25 % solvent B (0.1 % FA in 80 % acetonitrile) from 10 to 15 min and 25%–40 % solvent B from 15 to 40 min, with a 70 min total run time. The MS scan was done using detector: Orbitrap resolution 120000; scan range 350–1800 *m/z*; RF lens 30 %; AGC target 4.0 e5; maximum injection time 100 ms. The most intense ions with charge state 2–6 isolated in 3 s cycles were selected in the MS scan for further fragmentation. MS2 scan parameters set: activation HCD with 35 % normalized collision energy, detected at a mass resolution of 30000. The AGC target for MS/MS was set at 5.0 e4 and ion filling time set to 60 ms.

Hmp protein identification was performed by searching MS/MS data against the NCBI database in Proteome Discoverer (Thermo Fisher Sci, vs 2.5.), assuming digestion with the enzyme trypsin. The parameters for Sequest HT were set as follows: Enzyme: trypsin, Max missed cleavage: 2, Precursor mass tolerance: 10 ppm, Peptide tolerance: ±0.02 Da, Fixed modifications: carbamidomethyl (C); Dynamic modifications: oxidation (M), acetyl (N-term). The parameters for the Precursor ions quantifier were set as follows: peptides to use unique + razor, precursor abundance based on intensity; normalization mode: total peptide amount; scaling mode: on all average. Specific tryptic fragments of Hmp corresponding to the truncated and non-truncated parts of the protein were determined to distinguish between Hmp protein variants.

4.16. Statistical analysis

Statistical analysis was carried out by one-way analysis of variance (ANOVA) followed by Tukey's post-comparison test, Sidak's post-comparison test or a Student's *t*-test. All experiments were carried out with at least three biological replicates, and significance was assessed at *P* values of <0.05 (*), <0.005 (**), <0.0005 (***) and <0.00005 (****).

Declaration of competing interest

The authors declare that they have no known competing financial interests or personal relationships that could have appeared to influence the work reported in this paper.

Data availability

Data will be made available on request.

Acknowledgments

This work was funded by NIH/NIAID R01AI125588 and P01AI083211 Metabolomics Core to VCT, P01AI083211 Project 2 and Project 4 to PDF and TK, respectively. The EPR spectroscopy core is supported, in part, by an NIH Centers of Biomedical Research Excellence (COBRE) grant (1P30GM103335) awarded to the University of Nebraska's Redox Biology Center. The University of Nebraska Medical Center Mass Spectrometry and Proteomics Core Facility is administrated through the Office of the Vice Chancellor for Research and supported by state funds from the Nebraska Research Initiative (NRI). The funders had no role in the study design, data collection, interpretation, and decision to submit this work for publication. The authors have no conflict of interest to declare.

Appendix A. Supplementary data

Supplementary data to this article can be found online at https://doi.org/10.1016/j.redox.2023.102935.

References

[1] M. Otto, *Staphylococcus epidermidis*-the 'accidental' pathogen, Nat. Rev. Microbiol. 7 (8) (2009) 555–567.
[2] M. Widerstrom, Significance of *Staphylococcus epidermidis* in health care-associated infections, from contaminant to clinically relevant pathogen: this is a wake-up call, J. Clin. Microbiol. 54 (7) (2016) 1679–1681.
[3] L. Montanaro, P. Speziale, D. Campoccia, S. Ravaioli, I. Cangini, G. Pietrocola, S. Giannini, C.R. Arciola, Scenery of *Staphylococcus* implant infections in orthopedics, Future Microbiol. 6 (11) (2011) 1329–1349.
[4] F.C. Fang, Antimicrobial reactive oxygen and nitrogen species: concepts and controversies, Nat. Rev. Microbiol. 2 (10) (2004) 820–832.
[5] F.C. Fang, Nitric Oxide and Infection, Kluwer Academic/Plenum Publishers, New York, 1999.

[6] A.R. Richardson, S.J. Libby, F.C. Fang, A nitric oxide-inducible lactate dehydrogenase enables *Staphylococcus aureus* to resist innate immunity, Science 319 (5870) (2008) 1672–1676.

[7] S.S. Chaudhari, M. Kim, S. Lei, F. Razvi, A.A. Alqarzaee, E.H. Hutfless, R. Powers, M.C. Zimmerman, P.D. Fey, V.C. Thomas, Nitrite derived from endogenous bacterial nitric oxide synthase activity promotes aerobic respiration, mBio 8 (4) (2017).

[8] I. Gusarov, E. Nudler, NO-mediated cytoprotection: instant adaptation to oxidative stress in bacteria, Proc. Natl. Acad. Sci. U. S. A. 102 (39) (2005) 13855–13860.

[9] I. Gusarov, K. Shatalin, M. Starodubtseva, E. Nudler, Endogenous nitric oxide protects bacteria against a wide spectrum of antibiotics, Science 325 (5946) (2009) 1380–1384.

[10] K. Shatalin, I. Gusarov, E. Avetissova, Y. Shatalina, L.E. McQuade, S.J. Lippard, E. Nudler, *Bacillus anthracis*-derived nitric oxide is essential for pathogen virulence and survival in macrophages, Proc. Natl. Acad. Sci. U. S. A. 105 (3) (2008) 1009–1013.

[11] N.M. van Sorge, F.C. Beasley, I. Gusarov, D.J. Gonzalez, M. von Kockritz-Blickwede, S. Anik, A.W. Borkowski, P.C. Dorrestein, E. Nudler, V. Nizet, Methicillin-resistant *Staphylococcus aureus* bacterial nitric-oxide synthase affects antibiotic sensitivity and skin abscess development, J. Biol. Chem. 288 (9) (2013) 6417–6426.

[12] T.L. Kinkel, S. Ramos-Montanez, J.M. Pando, D.V. Tadeo, E.N. Strom, S.J. Libby, F. C. Fang, An essential role for bacterial nitric oxide synthase in *Staphylococcus aureus* electron transfer and colonization, Nat Microbiol 2 (2016), 16224.

[13] A.S. Arrow, H.W. Taber, Streptomycin accumulation by *Bacillus subtilis* requires both a membrane potential and cytochrome *aa3*, Antimicrob. Agents Chemother. 29 (1) (1986) 141–146.

[14] P.R. Gardner, A.M. Gardner, L.A. Martin, A.L. Salzman, Nitric oxide dioxygenase: an enzymic function for flavohemoglobin, Proc. Natl. Acad. Sci. U. S. A. 95 (18) (1998) 10378–10383.

[15] I.S. Bang, L. Liu, A. Vazquez-Torres, M.L. Crouch, J.S. Stamler, F.C. Fang, Maintenance of nitric oxide and redox homeostasis by the *Salmonella* flavohemoglobin hmp, J. Biol. Chem. 281 (38) (2006) 28039–28047.

[16] J. Membrillo-Hernandez, N. Ioannidis, R.K. Poole, The flavohaemoglobin (HMP) of *Escherichia coli* generates superoxide in vitro and causes oxidative stress in vivo, FEBS Lett. 382 (1–2) (1996) 141–144.

[17] D.M. Bodenmiller, S. Spiro, The *yjeB* (*nsrR*) gene of *Escherichia coli* encodes a nitric oxide-sensitive transcriptional regulator, J. Bacteriol. 188 (3) (2006) 874–881.

[18] D.A. Rodionov, I.L. Dubchak, A.P. Arkin, E.J. Alm, M.S. Gelfand, Dissimilatory metabolism of nitrogen oxides in bacteria: comparative reconstruction of transcriptional networks, PLoS Comput. Biol. 1 (5) (2005) e55.

[19] O. Soutourina, O. Poupel, J.Y. Coppee, A. Danchin, T. Msadek, I. Martin-Verstraete, CymR, the master regulator of cysteine metabolism in *Staphylococcus aureus*, controls host sulphur source utilization and plays a role in biofilm formation, Mol. Microbiol. 73 (2) (2009) 194–211.

[20] A.R. Richardson, P.M. Dunman, F.C. Fang, The nitrosative stress response of *Staphylococcus aureus* is required for resistance to innate immunity, Mol. Microbiol. 61 (4) (2006) 927–939.

[21] M. Pagels, S. Fuchs, J. Pane-Farre, C. Kohler, L. Menschner, M. Hecker, P. J. McNamarra, M.C. Bauer, C. von Wachenfeldt, M. Liebeke, M. Lalk, G. Sander, C. von Eiff, R.A. Proctor, S. Engelmann, Redox sensing by a Rex-family repressor is involved in the regulation of anaerobic gene expression in *Staphylococcus aureus*, Mol. Microbiol. 76 (5) (2010) 1142–1161.

[22] Y. Wu, Y. Wu, T. Zhu, H. Han, H. Liu, T. Xu, P. Francois, A. Fischer, L. Bai, F. Gotz, D. Qu, *Staphylococcus epidermidis* SrrAB regulates bacterial growth and biofilm formation differently under oxic and microaerobic conditions, J. Bacteriol. 197 (3) (2015) 459–476.

[23] Q. Ji, L. Zhang, F. Sun, X. Deng, H. Liang, T. Bae, C. He, *Staphylococcus aureus* CymR is a new thiol-based oxidation-sensing regulator of stress resistance and oxidative response, J. Biol. Chem. 287 (25) (2012) 21102–21109.

[24] C. Tanous, O. Soutourina, B. Raynal, M.F. Hullo, P. Mervelet, A.M. Gilles, P. Noirot, A. Danchin, P. England, I. Martin-Verstraete, The CymR regulator in complex with the enzyme CysK controls cysteine metabolism in *Bacillus subtilis*, J. Biol. Chem. 283 (51) (2008) 35551–35560.

[25] P.S. Novichkov, A.E. Kazakov, D.A. Ravcheev, S.A. Leyn, G.Y. Kovaleva, R. A. Sutormin, M.D. Kazanov, W. Riehl, A.P. Arkin, I. Dubchak, D.A. Rodionov, RegPrecise 3.0–a resource for genome-scale exploration of transcriptional regulation in bacteria, BMC Genom. 14 (2013) 745.

[26] X. Shu, Y. Shi, Y. Huang, D. Yu, B. Sun, Transcription tuned by S-nitrosylation underlies a mechanism for Staphylococcus aureus to circumvent vancomycin killing, Nat. Commun. 14 (1) (2023) 2318.

[27] K. Shatalin, E. Shatalina, A. Mironov, E. Nudler, H2S: a universal defense against antibiotics in bacteria, Science 334 (6058) (2011) 986–990.

[28] W. Shepard, O. Soutourina, E. Courtois, P. England, A. Haouz, I. Martin-Verstraete, Insights into the Rrf2 repressor family–the structure of CymR, the global cysteine regulator of Bacillus subtilis, FEBS J. 278 (15) (2011) 2689–2701.

[29] K.L. James, A.B. Mogen, J.N. Brandwein, S.S. Orsini, M.J. Ridder, M. A. Markiewicz, J.L. Bose, K.C. Rice, Interplay of nitric oxide synthase (NOS) and SrrAB in modulation of *Staphylococcus aureus* metabolism and virulence, Infect. Immun. 87 (2) (2019).

[30] G. Wu, H. Corker, Y. Orii, R.K. Poole, *Escherichia coli* Hmp, an "oxygen-binding flavohaemoprotein", produces superoxide anion and self-destructs, Arch. Microbiol. 182 (2–3) (2004) 193–203.

[31] Y. Orii, N. Ioannidis, R.K. Poole, The oxygenated flavohaemoglobin from *Escherichia coli*: evidence from photodissociation and rapid-scan studies for two kinetic and spectral forms, Biochem. Biophys. Res. Commun. 187 (1) (1992) 94–100.

[32] R.K. Poole, N.J. Rogers, A. D'Mello R, M.N. Hughes, Y. Orii, *Escherichia coli* flavohaemoglobin (Hmp) reduces cytochrome c and Fe(III)-hydroxamate K by electron transfer from NADH via FAD: sensitivity of oxidoreductase activity to haem-bound dioxygen, Microbiology (Read.) 143 (Pt 5) (1997) 1557–1565.

[33] N.J. Gilberthorpe, M.E. Lee, T.M. Stevanin, R.C. Read, R.K. Poole, NsrR: a key regulator circumventing Salmonella enterica serovar Typhimurium oxidative and nitrosative stress in vitro and in IFN-gamma-stimulated J774.2 macrophages, Microbiology (Read.) 153 (Pt 6) (2007) 1756–1771.

[34] D. Bruch-Gerharz, T. Ruzicka, V. Kolb-Bachofen, Nitric oxide and its implications in skin homeostasis and disease - a review, Arch. Dermatol. Res. 290 (12) (1998) 643–651.

[35] S.S. Chaudhari, V.C. Thomas, M.R. Sadykov, J.L. Bose, D.J. Ahn, M.C. Zimmerman, K.W. Bayles, The LysR-type transcriptional regulator, CidR, regulates stationary phase cell death in *Staphylococcus aureus*, Mol. Microbiol. 101 (6) (2016) 942–953.

[36] V. Winstel, P. Kuhner, B. Krismer, A. Peschel, H. Rohde, Transfer of plasmid DNA to clinical coagulase-negative staphylococcal pathogens by using a unique bacteriophage, Appl. Environ. Microbiol. 81 (7) (2015) 2481–2488.

[37] K.J. Livak, T.D. Schmittgen, Analysis of relative gene expression data using real-time quantitative PCR and the 2(-Delta Delta C(T)) Method, Methods 25 (4) (2001) 402–408.

[38] M.T. Forrester, C.E. Eyler, J.N. Rich, Bacterial flavohemoglobin: a molecular tool to probe mammalian nitric oxide biology, Biotechniques 50 (1) (2011) 41–45.

[39] S. Carfagna, C. Bottone, P.R. Cataletto, M. Petriccione, G. Pinto, G. Salbitani, V. Vona, A. Pollio, C. Ciniglia, Impact of sulfur starvation in autotrophic and heterotrophic cultures of the extremophilic microalga *Galdieria phlegrea* (*Cyanidiophyceae*), Plant Cell Physiol. 57 (9) (2016) 1890–1898.

[40] C. Wang, J. Lee, Y. Deng, F. Tao, L.H. Zhang, ARF-TSS: An alternative method for identification of transcription start site in bacteria, Biotechniques 52 (4) (2012).

[41] C.E. Heim, D. Vidlak, T. Kielian, Interleukin-10 production by myeloid-derived suppressor cells contributes to bacterial persistence during *Staphylococcus aureus* orthopedic biofilm infection, J. Leukoc. Biol. 98 (6) (2015) 1003–1013.